TISSUE ENGINEERING: Part A
Volume 21, Numbers 3 and 4, 2015

DOI: 10.1089/ten.tea.2014.0235

Adipose-Derived Stem-Cell-Seeded Non-Cross-Linked Porcine Acellular Dermal Matrix Increases Cellular Infiltration, Vascular Infiltration, and Mechanical Strength of Ventral Hernia Repairs

Tejaswi S. Iyyanki, MS, Lina W. Dunne, PhD, Qixu Zhang, MD, PhD, Justin Hubenak, BS, Kristin C. Turza, MD, and Charles E. Butler, MD, FACS

Adipose-derived stem cells (ASCs) facilitate wound healing by improving cellular and vascular recruitment to the wound site. Therefore, we investigated whether ASCs would augment a clinically relevant bioprosthetic mesh—non-cross-linked porcine acellular dermal matrix (ncl-PADM)—used for ventral hernia repairs in a syngeneic animal model. ASCs were isolated from the subcutaneous adipose tissue of Brown Norway rats, expanded, and labeled with green fluorescent protein. ASCs were seeded (2.5×10^4 cells/cm^2) onto ncl-PADM for 24 h before surgery. *In vitro* ASC adhesion to ncl-PADM was assessed at 0.5, 1, and 2 h after seeding, and cell morphology on ncl-PADM was visualized by scanning electron microscopy. Ventral hernia defects (2×4 cm) were created and repaired with ASC-seeded ($n = 31$) and control ($n = 32$) ncl-PADM. Explants were harvested at 1, 2, and 4 weeks after surgery. Explant remodeling outcomes were evaluated using gross evaluation (bowel adhesions, surface area, and grade), histological analysis (hematoxylin and eosin and Masson's trichrome staining), immunohistochemical analysis (von Willebrand factor VIII), fluorescent microscopy, and mechanical strength measurement at the tissue-bioprosthetic mesh interface. Stem cell markers CD29, CD90, CD44, and P4HB were highly expressed in cultured ASCs, whereas endothelial and hematopoietic cell markers, such as CD31, CD90, and CD45 had low expression. Approximately 85% of seeded ASCs adhered to ncl-PADM within 2 h after seeding, which was further confirmed by scanning electron microcopy examination. Gross evaluation of the hernia repairs revealed weak omental adhesion in all groups. Ultimate tensile strength was not significantly different in control and treatment groups. Conversely, elastic modulus was significantly greater at 4 weeks postsurgery in the ASC-seeded group ($p < 0.001$). Cellular infiltration was significantly higher in the ASC-seeded group at all time points ($p < 0.05$). Vascular infiltration was significantly greater at 4 weeks postsurgery in the ASC-seeded group ($p < 0.001$). The presence of ASCs improved remodeling outcomes by yielding an increase in cellular infiltration and vascularization of ncl-PADM and enhanced the elastic modulus at the ncl-PADM-tissue interface. With the ease of harvesting adipose tissues that are rich in ASCs, this strategy may be clinically translatable for improving ncl-PADM ventral hernia repair outcomes.

Introduction

Approximately 250,000 ventral hernia repairs are performed each year in the United States. Traditional hernia repair involves the direct closure of defects in the abdominal fascia, and the repair procedure has a recurrence rate of ~40%.[1–3] The use of meshes for the repair results in a lower recurrence rate of ~20%.[3,4] However, factors such as diabetes, infection, obesity, previous radiotherapy, previous chemotherapy, or complex oncologic defects can compromise wound healing at the repair site and increase the recurrence rate.

The ideal solution for reducing the recurrence of hernias is to facilitate the regeneration of the abdominal wall fascia tissue to its native healthy state.[5] Bioprosthetic meshes used for hernia repairs need to be able to withstand intra-abdominal pressure, quickly integrate into the native tissue at the repair site, and promote tissue regeneration.[5] Currently, the most common hernia repair meshes are synthetic meshes and acellular dermal matrices (ADMs).[6] Although

Department of Plastic Surgery, The University of Texas MD Anderson Cancer Center, Houston, Texas.

synthetic meshes such as polypropylene are useful, they elicit severe inflammatory responses and dense fibrous scar tissue formation that results in visceral adhesions; whereas the use of ADMs results in less inflammation, fewer adhesions, and lower risk of mesh infection.[7] Long-term clinical studies are currently evaluating the different types of ADMs used for ventral hernia repairs.[8]

Non-cross-linked porcine acellular dermal matrix (ncl-PADM) is an ADM commonly used for reconstructive surgical applications. Generally, PADMs have shown long-term utility in the repair of large, complex abdominal wall defects, especially in patients at high risk for healing complications.[9–13] Previous work by our group demonstrated that ncl-PADM becomes strongly integrated with native tissue at the tissue-bioprosthetic interface and results in very few and weak adhesions to the omentum in *in vivo* animal models.[14–16] Despite the advances in ADM repairs, hernia recurrence rates still remain high. Therefore, we sought to explore strategies to enhance the wound-healing response and promote tissue integration and the regeneration of abdominal wall fascia.

Adipose-derived stem cells (ASCs) have excellent regenerative capacity, and multiple studies have proved that they augment tissue repairs.[17–21] ASCs can be easily harvested from subcutaneous fat using liposuction, which negates the need for invasive biopsy techniques, such as those used in bone marrow tissue harvest.[22–26] ASCs also have the capacity to augment wound healing through improving neovascularization and cellular infiltration.[27–29] A previous study by our group showed that seeding ASCs onto ncl-PADM *in vivo* in a rat model increased vascularization and cellular infiltration at 2 weeks after surgery.[30] Since the success of hernia repairs depends on mechanical integrity at the repair site, the increase in cellular infiltration and vascularization by ASC incorporation may increase the native tissue integration into the bioprosthetic mesh, which would lead to an increase of mechanical strength at the interface. Therefore, we hypothesized that ASC-seeded ncl-PADM used in ventral hernia repairs *in vivo* would have greater mechanical properties at the mesh-tissue interface and greater cellular and vascular infiltration into the ADM than the control (unseeded) group.

Materials and Methods

Rat model and surgical technique

An established hernia repair model was used.[30] All animal use was conducted with the approval of The University of Texas MD Anderson Cancer Center Institutional Animal Care and Use Committee. Briefly, six syngeneic, inbred brown Norway rats (Charles River Laboratories, Wilmington, MA) underwent harvesting of subcutaneous adipose tissue for stem cell isolation and extraction. Sixty rats (200–250 g) underwent inlaid, bridged ventral hernia repair of 2×4 cm defects with ncl-PADM (Strattice; LifeCell Corp., Branchburg, NJ). Thirty-one rats received ASC-preseeded ncl-PADM, and 32 received ncl-PADM alone.

Isolation, culture, and labeling of rat ASCs

Subcutaneous fat tissue was harvested for ASC extraction.[30] Briefly, the fat tissue was minced and digested with a mixture of 0.075% type IA collagenase (Sigma, St. Louis, MO). The extracted cells were reconstituted in phosphate-buffered saline (PBS; Mediatech, Manassas, VA) with 1% bovine serum albumin (Fisher Scientific, Pittsburg, PA) and fixed with 1% paraformaldehyde (Electron Microscopy Sciences, Hatfield, PA) in PBS or cultured with α-minimum essential growth medium (Mediatech) containing 10% fetal bovine serum (Invitrogen, Carlsbad, CA), 2 mM L-glutamine, 100 μg/mL penicillin, and 100 μg/mL streptomycin (Invitrogen). Cells were cultured at 37°C and 5% CO_2 in a humidified incubator. Cells of passage number 1–4 were used in this study.

ASCs were transfected with a lentiviral vector carrying green fluorescent protein (GFP; Gentarget, San Diego, CA) using an adaptation of the method previously described.[30] Briefly, ASCs at 50% confluence in six-well tissue culture plates (BD, San Diego, CA) were incubated with 50 μL GFP vector mixed with 500 μL of growth medium for 24 h. 1.5 mL fresh growth medium was added after 24 h, and cells were further expanded and sorted using an Aria Cell Sorter (BD).

Flow cytometric characterization of ASCs

Cells were stained individually with the following antibodies for flow cytometry analysis (Table 1): hamster anti-CD29 (BD), mouse anti-CD44 (ABD Serotec, Raleigh, NC), mouse anti-CD90 (BioLegend, San Diego, CA), mouse anti-CD31 (BD), mouse anti-CD45 (BioLegend), and mouse anti-prolyl-4-hydroxylase-β (Novus, Littleton, CO). Composite stains of CD90-CD29, CD90-CD44, CD90-CD31, and CD90-CD45 were also prepared to further quantify coexpression of stem cell makers. Isotype negative controls were included. The data were interpreted with FlowJo software (v 7.6.5; TreeStar, Inc., Ashland, OR).

In vitro *cell adhesion evaluation*

ASCs were seeded onto ncl-PADM scaffolds of 6 mm diameter at 25,000 cells/cm^2 in a 96-well plate, and cultured for 0.5, 1, and 2 h ($n = 3$). ASC-seeded ncl-PADM scaffolds were transferred to a different well for a gentle PBS rinse after incubation. All the supernatant media were collected from each well where unattached cells were counted using a Z1 Coulter Counter (Beckman Coulter, Brea, CA). Cells that were collected in the final supernatant from each well were subtracted from the initial seeded cell number to obtain the percentage of cells adherent to the scaffold. Tissue culture plates ($n = 3$) seeded with ASCs were used as a control for comparisons.

Table 1. Description of Selected Antibodies for Characterization of Rat Adipose-Derived Stem Cells

Antibody	*Stem cell expression*	*Description*	*References*
CD31	− −	Endothelial cell marker	22,34,35
CD45	− −	Hematopoietic cell marker	22,35,36
CD29	+ +	Adhesion	35,36
CD44	+ +	Adhesion	35,36
CD90	+ +	Stromal cell marker	22,25,35
P4HB	+ +	Fibroblast antigen	37

Note: − − denotes low expression and + + denotes high expression.

Scanning electron microscopy evaluation of cell morphology

Ncl-PADM scaffolds seeded with ASCs (25,000 cells/cm^2) and cultured for 1, 2, and 3 h and 1 day underwent scanning electron microscopy analysis. Samples were fixed with PBS containing 3% gluteraldehyde (Polysciences, Warrington, PA) and 2% paraformaldehyde (USB, Fremont, CA) and washed in 0.1 M cacodylate buffer, pH 7.3 (Ted Pella, Inc., Redding, CA), and distilled water before drying. Samples were then dehydrated by adding a series of increasing concentrations of ethanol followed by hexamethyldisilazane for 5 min each and finally air dried overnight. Samples were mounted, coated with 25 nm of platinum alloy under a vacuum using a Balzer MED 010 evaporator (Technotrade International, Manchester, NH), and then immediately flash carbon-coated under the vacuum. Samples were transferred to desiccators and then examined with a JSM-5910 scanning electron microscope (JEOL, USA, Inc., Peabody, MA) at an accelerating voltage of 5 kV.

Implant preparation and seeding

Ncl-PADM was cut into 2×4–cm pieces in a sterile fashion. The ASC-preseeded ncl-PADM scaffolds containing GFP$^+$ ASCs at a density of 25,000 cells/cm^2 were cultured for 24 h before surgical implantation. Ncl-PADM was implanted into the rats with the ASC-preseeded side facing the musculofascia and skin.

Gross evaluation and histological analysis

Rats were euthanized by CO_2 asphyxiation at 1, 2, and 4 weeks after surgery. The entire abdominal wall, including the repair site, was exposed in a manner similar to that previously reported,[11,14,15] and the repair integrity was grossly and histologically assessed as previously described.[11,14,15,30]

For gross evaluation, the abdominal wall was excised, and the peritoneal cavity was exposed. The size (percentage of reconstructed area), type (omentum and intestine), and strength (grade) of adhesions were recorded. Adhesion strength was graded using the established Butler Adhesion Scale.[7,31,32] Zero represents no adhesion, 1 represents adhesions freed easily with gentle tension, 2 represents adhesions freed with blunt dissection, and 3 represents adhesions requiring sharp dissection.

Cross-sectional specimens that included ncl-PADM and the surrounding native musculofascia and skin were excised for histological and immunohistochemical analysis. Tissue sections underwent hematoxylin and eosin and trichrome staining for examination of tissue architecture and cellular infiltration, as previously described.[30] Tissue sections were also stained for von Willebrand factor VIII (A0082, rabbit anti-human, 1:100; Dako, Glostrup, Denmark).

Based on Masson's trichrome staining, cellular infiltration was quantified by outlining the total cell-containing area with Adobe Photoshop CS3 (Adobe, San Diego, CA) and expressed as a percentage of the total mesh implant. Images were taken using an Olympus microscope with a 4× objective (Olympus, Philadelphia, PA). Images were digitally merged to show the entire abdominal wall cross-section. Sections stained with anti-von Willebrand factor VIII were used for analyzing vascularization. Image series were taken under a microscope at 20× magnification to obtain the total count of vascular structures for the entire tissue section. Sections imaged separately at 4× magnification and digitally merged using Adobe Photoshop CS3 were used to obtain the total area of the tissue section. Vessel density was defined as the number of vessels in the total area.

Mechanical testing

Two transverse sections (3×0.5 cm) per animal were used for mechanical testing at the implant-tissue interface as

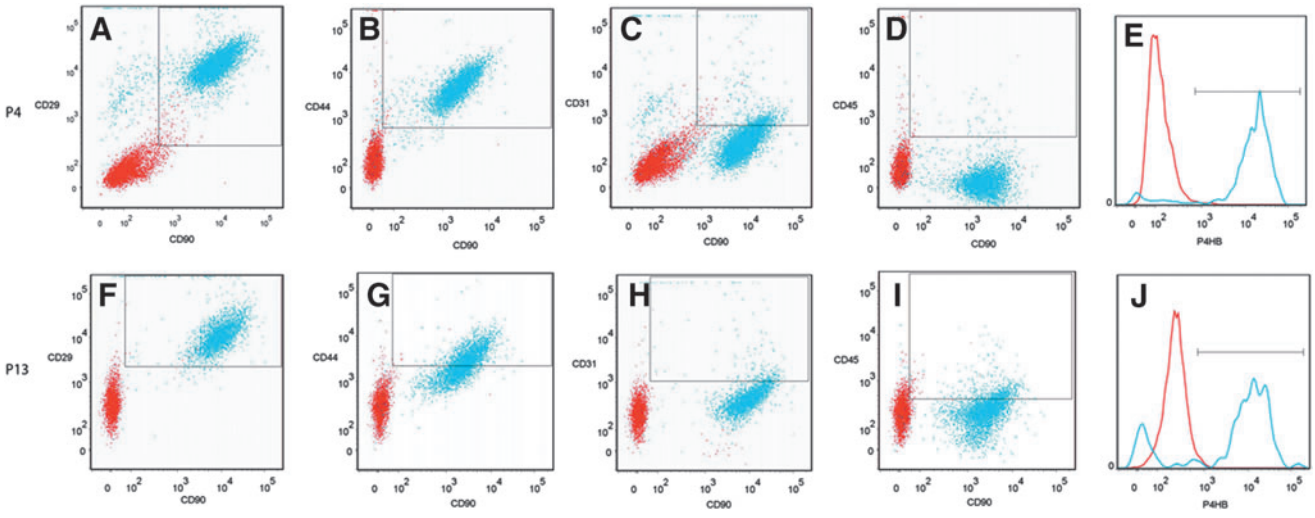

FIG. 1. Representative analysis of stained cells isolated from cultured rat adipose tissue at P4 **(A–E)** and P13 **(F–J)** passages analyzed by fluorescence-assisted cell sorting. P4: **(A)** 96.0% of cultured adipose-derived stem cells (ASCs) expressed both CD29 and CD90, **(B)** 97.9% of the cells expressed CD44 and CD90, **(C)** 9.7% expressed both CD31 and CD90, **(D)** 1.1% expressed both CD45 and CD90, and **(E)** 96.1% expressed prolyl 4-hydroxylase, beta (P4HB). P13: **(F)** 97.5% of cultured ASC expressed both CD29 and CD90, **(G)** 54.7% of the cells expressed CD44 and CD90, **(H)** 7.9% expressed both CD31 and CD90, **(I)** 15.8% expressed both CD45 and CD90, and **(J)** 78.3% expressed P4HB. Color images available online at www.liebertpub.com/tea

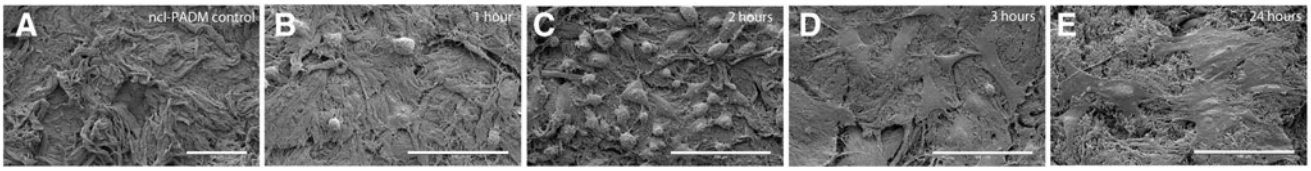

FIG. 2. **(A)** Non-cross-linked porcine acellular dermal matrix (ncl-PADM) control without ASCs shows the fibrous structure of the native extracellular matrix. **(B–E)** Representative electron microscopy images of cultured ASC on ncl-PADM tissue at various culture times. **(B)** Initial ASC attachment with a round morphology was seen within 1 h after seeding. **(C)** At 2 h, cells attached and started spreading out on the ncl-PADM. **(D)** ASCs developed a spindle-like morphology by 3 h after seeding. **(E)** Cells continued to spread out at 24 h after seeding and developed further striations. Scale bar = 100 μm.

previously described.[30] Briefly, one clamp was placed on the musculofascia and the other clamp was placed over the implant area so that the interface was between the two clamps. Uniaxial tensile strain was applied with a 250-N-load cell (Transducer Technologies, Temecula, CA) at a 500-mm/s strain rate at room temperature. The stress–strain curves were obtained to derive the ultimate tensile strength and elastic modulus.

Statistical analysis

Statistical analysis was carried out using Sigma Stat 3.0 (Aspire Software International, Ashburn, VA). Two-way analysis of variance was performed to determine the effects of the treatment group (ASC-seeded vs. control ncl-PADM), time of specimen harvest (1, 2, or 4 week), and interaction between the treatment and time course. All other pair-wise multiple comparisons were made using the Holm–Sidak method. Values of $p < 0.05$ were defined as statistically significant.

Results

Isolation, characterization, and GFP transfection

Fluorescence-assisted cell sorting analysis of cultured ASCs at passage 4 (P4) and P13 (Fig. 1) revealed high coexpression of the cell surface antigens listed in Table 1 and high specificity for known adipose stem cell markers, including cell adhesion markers. At P4, 96.0% of cells were $CD29^+$ and $CD90^+$ (Fig. 1A), 97.9% were $CD44^+$ and $CD90^+$ (Fig. 1B), and 96.1% were prolyl 4-hydroxylase, beta $(P4HB)^+$ (Fig. 1E). Endothelial (CD31) and hematopoietic (CD45) cell markers had low specificity: 9.7% of P4 cells were $CD31^+$ and $CD90^+$ (Fig. 1C), and 1.1% were $CD45^+$ and $CD90^+$ (Fig. 1D). Continued expression of the stem cell markers was seen even at P13: 97.5% of cells were $CD29^+$ and $CD90^+$ (Fig. 1F), 54.7% were $CD44^+$ and $CD90^+$ (Fig. 1G), and 78.3% were $P4HB^+$ (Fig. 1J). CD31 and CD45 expression remained low: 7. 9% of cells were $CD31^+$ and $CD90^+$ (Fig. 1H), and 15.8% were $CD45^+$ and $CD90^+$ (Fig. 1I).

Scanning electron microscopy evaluation of cell morphology

ASC morphology was visualized on ncl-PADM with electron microscopy (Fig. 2). Ncl-PADM controls without cells showed organized fibrous bundle topography in the native extracellular matrix (Fig. 2A). Initial ASC attachment was seen within 1 h after seeding, as evidenced by the cells' round morphology (Fig. 2B). At 2 h, the attached cells started to spread out and flatten on the ncl-PADM (Fig. 2C). ASCs developed a spindle-like morphology by 3 h after seeding (Fig. 2D) and retained a flat morphology at 24 h after seeding with further development of striations that indicated the establishment of cell adhesion (Fig. 2E).

In vitro *evaluation of ASC adhesion to ncl-PADM*

ASCs percent adhesion to ncl-PADM was quantified and compared with percent adhesion to a tissue culture plate within the first 2 h of seeding (Fig. 3). ASC adhesion to ncl-PADM was initially at 92% ± 0.1% at 0.5 h after seeding and decreased to 70% ± 0.1% ($p < 0.05$) at 1 h followed by an increase to 85% ± 0.1% ($p < 0.05$) by 2 h. A similar trend was seen for the tissue culture plate with 82% ± 0.0% adhesion at 30 min followed by a decrease at 1 h to 70% ± 0.0% ($p < 0.05$) and an increase to 85% ± 0.0% ($p < 0.05$) at 2 h after seeding. There were no significant differences in the adhesion rates between the control tissue culture plate and

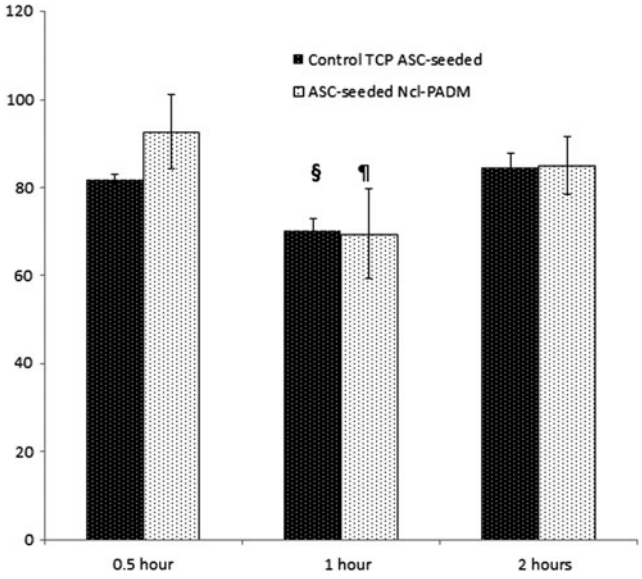

FIG. 3. Quantitative analysis of ASC adhesion to ncl-PADM and control tissue culture plate (TCP) at various culture times *in vitro*. $^{¶}p < 0.05$ compared with ncl-PADM 0.5 h and ncl-PADM 2 h. $^{§}p < 0.05$ compared with control 0.5 h and control 2 h. Errors bars shown refer to standard deviation.

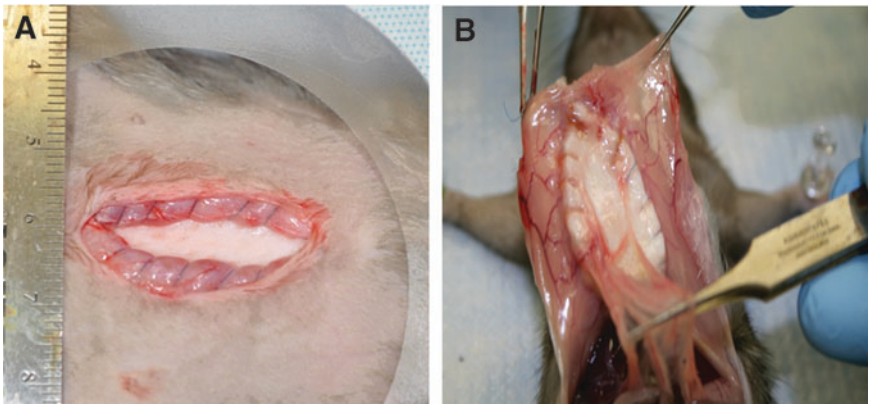

FIG. 4. **(A)** Representative images of inlay-acute ventral hernia repair surgical model. ASC-seeded ncl-PADM meshes were implanted with the ASC side facing out toward the muscle and ncl-PADM interface. **(B)** Ncl-PADM meshes were evaluated for adhesion type, area, and grade. Representative image shows benign omental adhesions. Color images available online at www .liebertpub.com/tea

ncl-PADM groups at any of the incubation times, but the rate for ASC-seeded ncl-PADM at 1 h was significantly lower than that at 30 min and 2 h ($p < 0.05$).

Gross evaluation of ventral hernia repair

The *in vivo* model validated in our pilot study[30] mimics the clinical setting for adipose tissue stromal vascular fraction repair of ventral hernias. Ncl-PADM meshes were implanted in the animals using inlay ventral hernia repair (Fig. 4A). Gross evaluation of the ncl-PADM mesh explants demonstrated only weak omental adhesions to the repair site, and there were no intestinal adhesions to the repair site in any animal. All implants retained their integrity with no signs of evisceration, herniation, or bowel adhesions to the implants (Fig. 4B). The area, grade, and type of adhesion are summarized in Table 2. Adhesion area seen in both groups was significantly larger at 1 week than at 2 ($p = 0.005$) and 4 ($p = 0.013$) weeks after surgery. No significant difference was found in adhesion grade (strength) between the ASC-seeded ncl-PADM and control ncl-PADM at 1, 2, or 4 weeks.

Mechanical strength

Mechanical strength, including ultimate tensile strength and elastic modulus, was evaluated at the interface between ncl-PADM and the native animal tissue. Representative stress–strain curves of ASC-seeded ncl-PADM and ncl-PADM controls at 1, 2, and 4 week are shown in Figure 5A. Elastic modulus and ultimate tensile strength were obtained from the stress–strain curves for further comparisons.

Ultimate tensile strength was significantly associated with time (Fig. 5B). Although mean ultimate tensile strength was greater in ASC-seeded ncl-PADM at 2 and 4 weeks than in the ncl-PADM control at 2 and 4 weeks, respectively, UTS was not significantly associated with treatment (ASC-seeded vs. control ncl-PADM) at any time point. At 4 weeks after surgery, the ultimate tensile strengths of both the control and ASC-seeded ncl-PADM were significantly greater than that of the ASC at 1 and 2 weeks after surgery ($p < 0.001$ each).

However, the elastic modulus was significantly associated with treatment (ASC-seeded vs. control ncl-PADM, $p = 0.038$), time of harvest (4 weeks vs. 1 or 2 weeks, $p < 0.001$), and their interactions ($p = 0.002$). Elastic modulus was significantly greater ($p < 0.001$) in the ASC-seeded ncl-PADM at 4 weeks than in the ncl-PADM control at 4 weeks, as shown in Figure 5C.

Histological evaluation

Explanted ncl-PADM stained with Masson's trichrome was divided into regions, as shown in Figure 6A. Cellular infiltration was seen in all the regions as early as 1 week and persisted through weeks 2 and 4. Representative images of control and ASC-seeded ncl-PADM at 4 weeks are shown in Figure 6B, and quantification of infiltration is shown in Figure 6C. Cellular infiltration was significantly associated with ASC treatment, but neither with the time of harvest nor with their interactions. Cellular infiltration was significantly greater in ASC-seeded ncl-PADM than in controls ($p = 0.013$), as illustrated by Figure 6C.

Table 2. Gross Evaluation of Adhesions in Ventral Hernia Repair at Weeks 1, 2, and 4

	Control group (n = *32*)			*ASC group* (n = *31*)		
Harvest time	*Type of adhesion* (n)	*Adhesion area (%)*	*Adhesion grade*	*Type of adhesion* (n)	*Adhesion area (%)*	*Adhesion grade*
1 week	Omental (10)	20.5 ± 27.5^a	0.64 ± 0.50^a	Omental (8)	21.4 ± 26.2^a	0.41 ± 0.30^a
2 week	Omental (3)	2.8 ± 7.8^b	0.30 ± 0.63^b	Omental (4)	2.9 ± 6.2^b	0.40 ± 0.66^b
4 week	Omental (5)	4.2 ± 8.8^c	0.45 ± 0.57^c	Omental (5)	7.5 ± 12.5^c	0.50 ± 0.67^c

Data describing adhesion area and adhesion grade are mean percent area ± standard deviations and mean ± standard deviations, respectively, unless otherwise specified.

[a] $n = 11$ and 11 for control and ASC group harvested at 1 week, respectively.

[b] $n = 10$ and 10 for control and ASC group harvested at 2 weeks, respectively.

[c] $n = 11$ and 10 for control and ASC group harvested at 4 weeks, respectively.

ASC, adipose-derived stem cell.

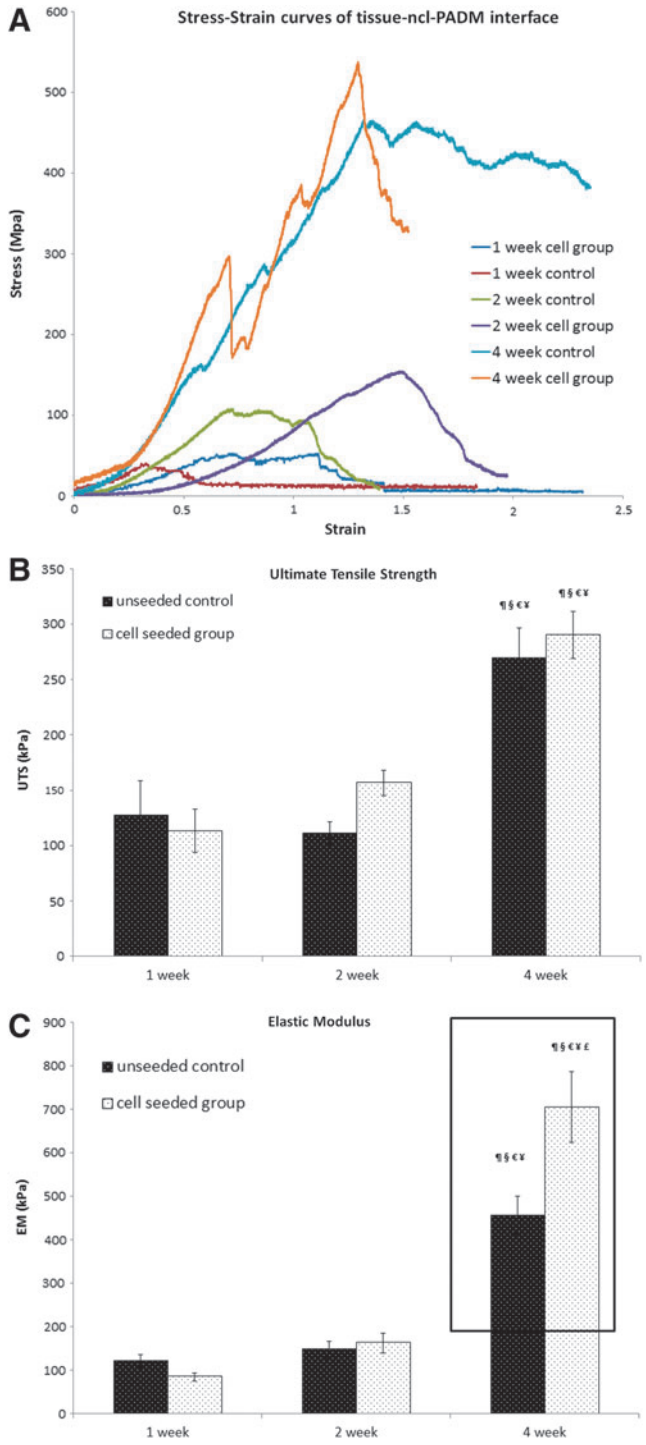

FIG. 5. **(A)** Representative stress–strain curves of the native tissue-mesh interface for control and ASC-seeded ncl-PADM meshes at 1, 2, and 4 weeks. **(B)** Ultimate tensile strength of the interface. **(C)** Elastic modulus of the interface. $^{¶}p<0.05$ compared with 1 week cell group, $^{§}p<0.05$ compared with 1 week control, $^{€}P<0.05$ compared with 2 week control, $^{¥}p<0.05$ compared with 2 week cell group, and $^{£}p<0.05$ compared with 4 week control. Errors bars shown refer to standard deviation. Color images available online at www.liebertpub.com/tea

Immunohistochemical analysis of hernia repair

Representative von Willebrand factor VIII-stained sections were identified for positively stained vascular structures (Fig. 7A, black arrows) of control and ASC-seeded ncl-PADM at 1, 2, and 4 weeks. Vascular densities were then quantified and compared (Fig. 7B). The level of vascular infiltration was significantly associated with the treatment (ASC-seeded vs. control ncl-PADM, $p<0.001$), time of harvest (4 weeks vs. 1 or 2 weeks, $p<0.001$), and their interactions ($p<0.001$). Vascular infiltration at 1, 2, and 4 weeks (number of vessels/mm^2) was 1.66 ± 1.21/mm^2, 1.29 ± 0.45/mm^2, and 5.48 ± 3.79/mm^2, respectively, in control ncl-PADM and 1.57 ± 1/mm^2, 2.57 ± 0.91/mm^2, and 13.03 ± 4.34/mm^2, respectively, in ASC-seeded ncl-PADM. Vascular infiltration was significantly greater in ASC-seeded ncl-PADM than in control ncl-PADM at 4 weeks (Fig. 7B; $p<0.001$). Vascular infiltration showed an increasing trend from 1 week through 4 week in both treatment groups. For example, in the ASC-seeded ncl-PADM group, vascular infiltration was significantly greater at 4 weeks than at 1 week ($p<0.001$) and 2 weeks ($p<0.001$).

GFP visualization of implanted ASCs

To verify the presence of implanted ASCs expressing GFP, fluorescence imaging of ASC-seeded ncl-PADM was performed at 2 weeks. Blue 2-(4-amidinophenyl)-1H-indole-6-carboxamidine counter-stain was used to visualize the cell nucleus. GFP$^+$ ASCs were found at 2 weeks, but not at 4 weeks (results at 4 weeks not shown) in tissue sections of bioprosthetic meshes, as shown in Figure 8.

Discussion

In this study, rat ASCs were isolated from subcutaneous adipose tissue and seeded onto ncl-PADM for ventral hernia repair. ASCs (GFP$^+$) on implants survived for at least 2 weeks and persisted through the critical stages of wound repair. Gross evaluation showed weak omental adhesions with ASC seeding and no differences in the area and grade (strength) of adhesion between ASC-seeded and control groups. Mechanical profiles, notably elastic modulus, were found to be greater in the ASC-seeded group at 4 weeks. Cellular infiltration was significantly greater in the ASC-seeded group at all the time points studied (1, 2, and 4 weeks), while vascular infiltration was greater in the ASC-seeded group at 4 weeks. A significant improvement in remodeling outcomes of hernia repairs (such as cellular infiltration, vascularization, and mechanical strength) is beneficial for rapid integration of meshes into the surrounding tissue.

Autologous cell transplantation is ideally preferred compared with xenograft and allograft transplantation to avoid inflammation and rejection. Therefore, a syngeneic rat model was utilized in this study instead of using ASCs from humans or GFP-expressing transgenic mice. The use of ASCs from humans or GFP-expressing transgenic mice may necessitate the use of immunodeficient rats to avoid immune system rejection of the transplanted ASCs,[33] thereby significantly shifting the focus away from the studying normal wound-healing response that is essential for the hernia repair model.

The flow cytometric surface profile characteristics of ASCs in our study were found to be consistent with those of

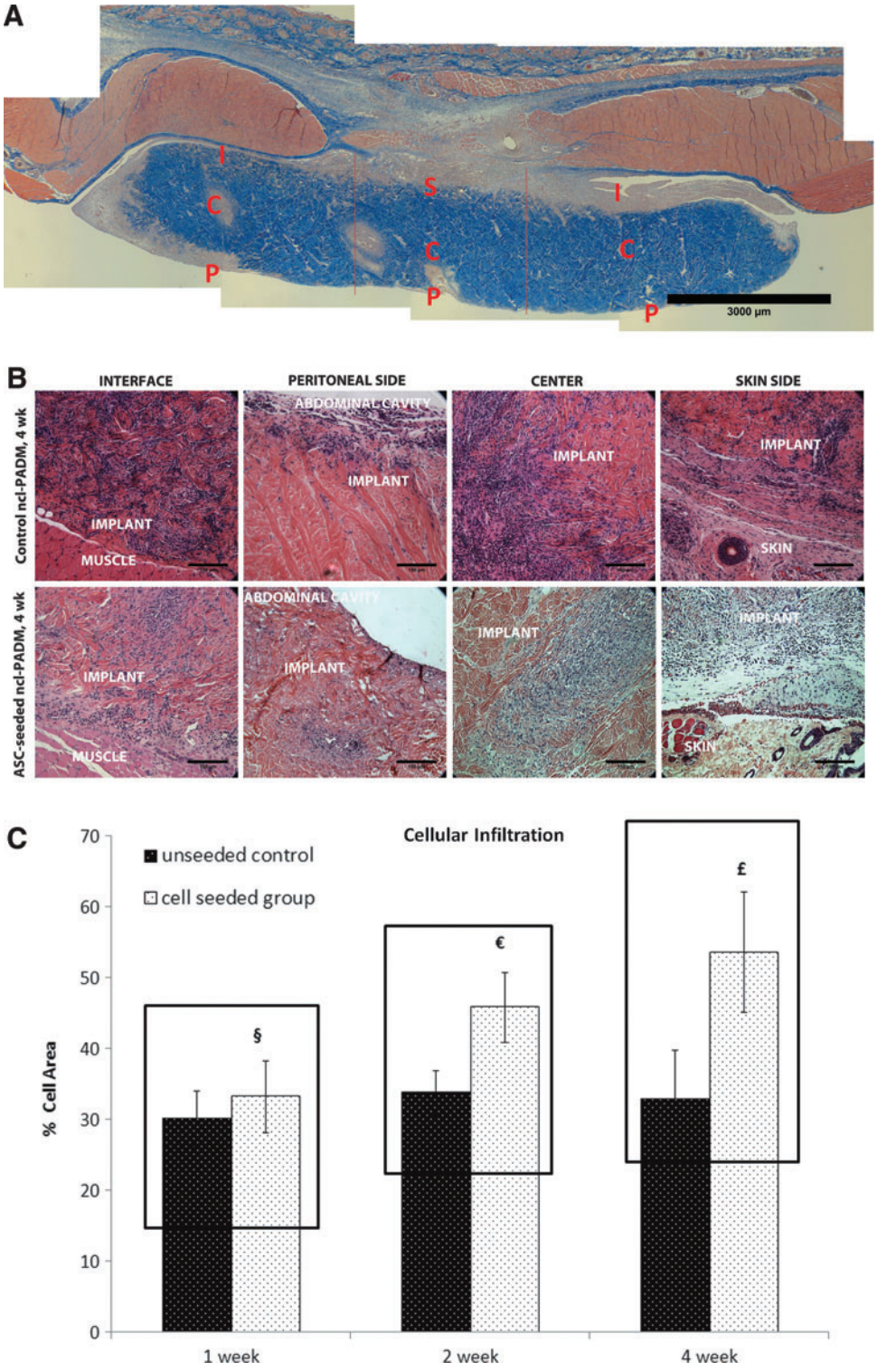

FIG. 6. **(A)** Representative image of Masson's trichrome stain of ASC-seeded ncl-PADM explant. Regions labeled are the peritoneal side (P), center (C), skin (S), and interface (I) of native muscular tissue and ncl-PADM implants. **(B)** Representative images of hematoxylin and eosin-stained slides showing cellular infiltration (blue marble stain) in ncl-PADM implants at 4 weeks at the interface, peritoneal side, center, and skin side. **(C)** Quantification of cellular infiltration of ncl-PADM in hernia repairs at 1, 2, and 4 weeks. $^{\S}p<0.05$ compared with 1 week control, $^{€}p<0.05$ compared with 2 week control, and $^{£}p<0.05$ compared with 4 week control. Errors bars shown refer to standard deviation. Color images available online at www.liebertpub.com/tea

other studies,[22,25,34–37] and the ASCs were found to have a high degree of purity. Our *in vitro* data, including ASC adhesion and scanning electron micrographs, suggest that ASCs established attachment within 2 h after plating on an ncl-PADM bioprosthetic mesh and spread out within 4–24 h. ASC adherence on ncl-PADM mesh is critical to make this system feasible for clinical translation. The natural environment of ncl-PADM's fibrous architecture and chemistry may support ASC adhesions, as suggested by our data and other studies.[38] Therefore, 4–24 h is a reasonable amount of time to allow ASCs to attach onto meshes before implantation.

The role of ASCs in regenerative wound healing[39–41] has been established and is currently being avidly explored. Wound healing occurs in stages that include inflammatory cell infiltration, collagen deposition, vascularization, and

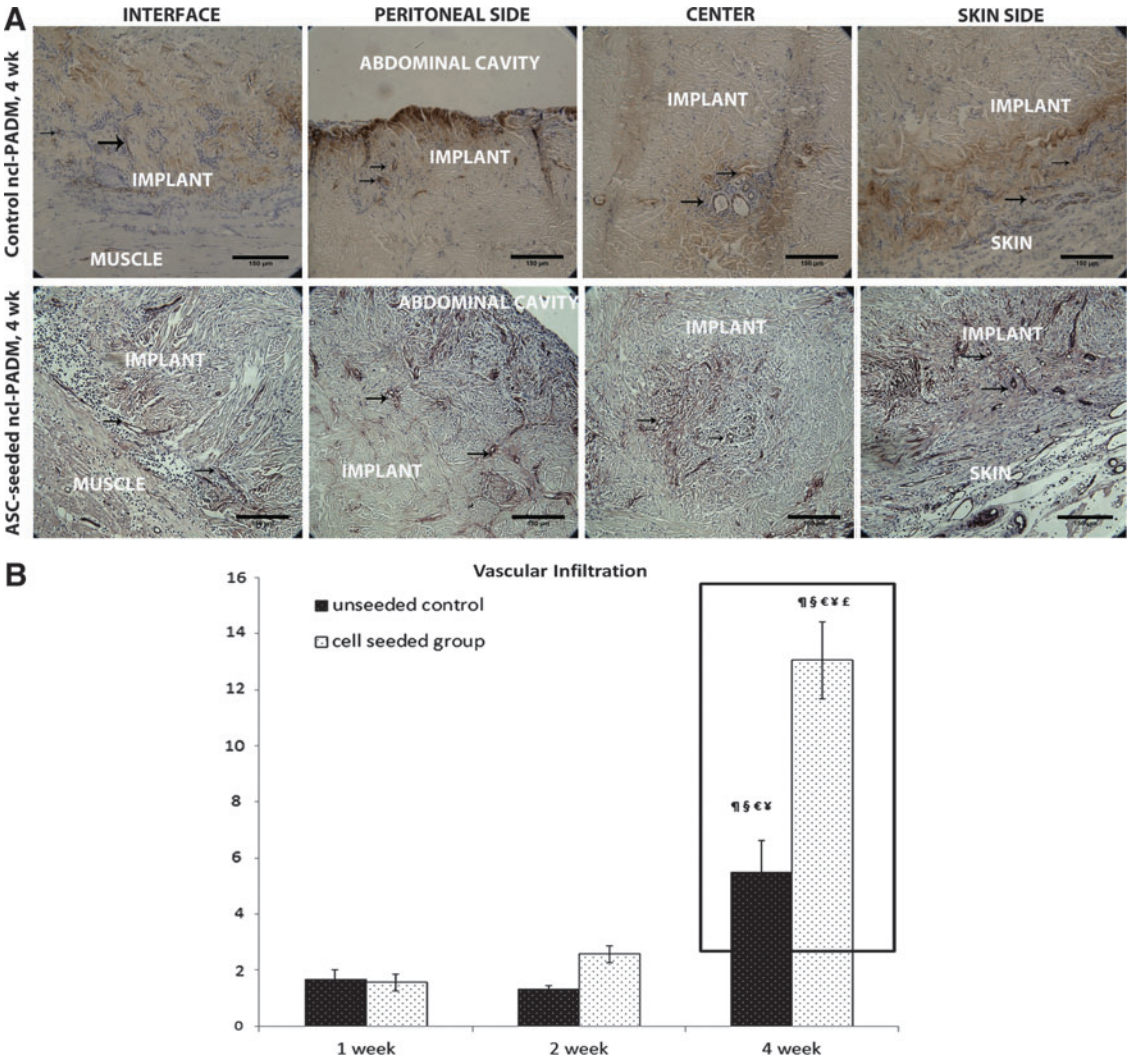

FIG. 7. **(A)** Representative images of von Willebrand factor VIII staining showing vascular structures (brown stain; *black arrows*) in ncl-PADM explants at 4 week in hernia repairs at the interface, peritoneal side, center, and skin side. **(B)** Vascular infiltration was measured by vessel density (number of vessels/mm^2) in ncl-PADM hernia repairs at 1, 2, and 4 week. $^{¶}p < 0.05$ compared with 1 week cell group, $^{§}p < 0.05$ compared with 1 week control, $^{€}p < 0.05$ compared with 2 week control, $^{¥}p < 0.05$ compared with 2 week cell group, and $^{£}p < 0.05$ compared with 4 week control. Errors bars shown refer to standard deviation. Color images available online at www.liebertpub.com/tea

remodeling.[42] Recent studies have shown that inflammation is essential for regenerative wound healing and is determined by macrophage phenotypes at various stages of wound healing.[43–45] Other studies have shown that ASC-mediated wound healing decreases inflammation.[46,47] Our previous studies have shown that seeded or injected ASCs were found to proliferate in several wound-healing models where they differentiate into tissue-specific cell types and promote the host-tissue cellular infiltration and vascularization of wounds.[30,40,41] An increase in cellular infiltration

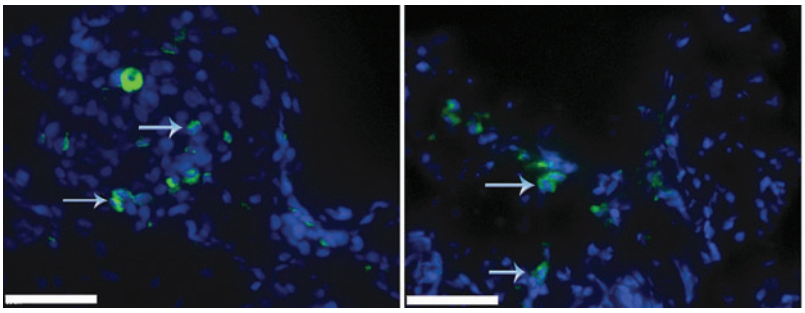

FIG. 8. Green fluorescent protein (GFP)-positive ASCs (*green*) were visualized under the fluorescent microscope at 2 week in ASC-seeded ncl-PADM implants. *Blue arrows* in the image point to GFP$^+$ cells. Blue color staining [2-(4-amidinophenyl)-1H-indole-6-carboxamidine] shows cellular nuclei. Scale bar = 50 μm. Color images available online at www.liebertpub.com/tea

and vascularization is also desired in hernia repairs in order to minimize infectious complications with adequate blood flow and efficient pathogen removal. Our histology evaluation of cellular and vascular infiltration supports the ability of ASCs to augment tissue regeneration in ventral hernia repairs. Early remodeling parameters such as cellular infiltration, vascular infiltration, and elastic modulus were significantly improved with ASC treatment. Furthermore, the tracing of GFP-labeled ASCs at the repair site and the significant improvements in the remodeling outcomes suggested that the implanted ASCs may aid in this.

Bowel adhesions in hernia repairs with synthetic meshes are a major problem, which can be reduced by using bioprosthetics, including ncl-PADM and others.[9–13] Therefore, the particular increase in cellular infiltration and vascularization in our study without an increase in bowel adhesion to ncl-PADM is a highly desirable outcome (Table 2). Increase in elastic modulus but not in ultimate tensile strength may suggest the role of ASCs in effective wound healing. Since the elastic modulus of ncl-PADM mesh is greater than that of the rat abdominal wall musculofascia, better integration of ncl-PADM into surrounding native tissue would increase the elastic modulus of the composite at the interface, as per the rule of composite mixtures according to the Voigt model.[48] It is possible that an increase in the rate of ultimate tensile strength due to ncl-PADM incorporation may be lower than the rate of increase in elastic modulus by 4 weeks. Hence, long-term evaluations at 2 or 3 months in our future studies will help further shed some light on ultimate tensile strength development over time. Therefore, a combination of increased elastic modulus, cellular infiltration, and vascularization, but not bowel adhesions, may suggest superior early integration of mesh and remodeling at the interface due to the action of stem cells.

Similar synergistic effects have been seen with the incorporation of different types of cells at the repair site in various wound-healing models[39–41] and, in particular, in hernia repairs and laparotomies.[30,49,50] For instance, Xing *et al.*[50] used amnion-derived progenitor cells in laparotomies, and Zhao *et al.*[49] used bone marrow-derived mesenchymal stem cells seeded onto decellularized dermal scaffolds in abdominal wall repairs. We have also previously used rat-derived ASCs to show enhanced cellularization and vascularization at 2 weeks in hernia repairs.[30] Despite the different types of cells the authors used, the synergistic wound-healing effects of the cells were similar to those observed in the current study using ASCs. However, the use of ASCs has a significant advantage because of their ease of access and minimal regulatory concerns. ASCs can be extracted using a relatively low-risk surgical procedure from subcutaneous adipose tissue, which is routinely discarded in liposuction procedures. Since autologous fat transplantation is also a routine clinic procedure, the use of cells isolated from this tissue for transplantation raises fewer safety concerns than does the use of other cells.[51] Therefore, ASCs could be a source of multipotent stem cells for use in several types of reconstructive surgeries.

In ventral hernia repair, musculofascial regeneration to replace the lost or compromised native tissue is the goal. Early remodeling indicated by greater elastic modulus and increased cellular infiltration and vascular infiltration with the use of ASC-seeded ncl-PADM compared with unseeded controls potentially improves the likelihood of better long-term outcomes. However, cross-species translation is essential in any preclinical translational research, and our results require validation.[52] Therefore, it is important to show the efficacy of these stem cells for ventral hernia repairs in a large animal model. This study may serve as a foundation for future investigations of the pre-clinical and clinical use of ASCs in complex reconstructive procedures such as ventral hernia repair.

Conclusion

We have performed a preclinical evaluation of ASCs for ncl-PADM-mediated ventral hernia repair, and the results showed that the use of ASC-seeded bioprosthetic mesh improved the cellular infiltration, vascular infiltration, and mechanical strength at the tissue-to-mesh interface for hernia repair in the early remodeling stages. Future studies will be required to evaluate the long-term remodeling outcomes with the use of ASCs in abdominal wall reconstruction. Our findings provide the proof of concept that ASCs can be harvested in the clinical setting via lipo-aspiration and reinjected during reconstructive surgery to improve hernia repair outcomes.

Acknowledgments

The authors would like to acknowledge the MD Anderson Cancer Center Core Grant CA016672 for electron microscopy, flow cytometry, and histology services. This research was supported in part by the Kyte Foundation and a grant from the Plastic Surgery Foundation (ASRM/PSF Combined Pilot Research Grant, ID 175775). The authors thank Zach Bohannan and Dawn Chalaire for their scientific editing services.

Disclosure Statement

No author has anything to disclose related to this work.

References

1. Stoppa, R.E. The treatment of complicated groin and incisional hernias. World J Surg **13,** 545, 1989.
2. Hesselink, V.J., Luijendijk, R.W., de Wilt, J.H., Heide, R., and Jeekel, J. An evaluation of risk factors in incisional hernia recurrence. Surg Gynecol Obstet **176,** 228, 1993.
3. Luijendijk, R.W., Hop, W.C., van den Tol, M.P., de Lange, D.C., Braaksma, M.M., Ijzermans, J.N., *et al.* A comparison of suture repair with mesh repair for incisional hernia. N Engl J Med **343,** 392, 2000.
4. Heniford, B.T., Park, A., Ramshaw, B.J., and Voeller, G. Laparoscopic repair of ventral hernias: nine years' experience with 850 consecutive hernias. Ann Surg **238,** 391, 2003.
5. Falco, E.E., Roth, J.S., and Fisher, J.P. Skeletal muscle tissue engineering approaches to abdominal wall hernia repair. Birth Defects Res C Embryo Today **84,** 315, 2008.
6. Butler, C.E. The role of bioprosthetics in abdominal wall reconstruction. Clin Plast Surg **33,** 199, 2006.
7. Butler, C.E., and Prieto, V.G. Reduction of adhesions with composite AlloDerm/polypropylene mesh implants for abdominal wall reconstruction. Plast Reconstr Surg **114,** 464, 2004.
8. Shah, B.C., Tiwari, M.M., Goede, M.R., Eichler, M.J., Hollins, R.R., McBride, C.L., *et al.* Not all biologics are equal! Hernia **15,** 165, 2011.

9. Nemeth, N.L., and Butler, C.E. Complex torso reconstruction with human acellular dermal matrix: long-term clinical follow-up. Plast Reconstr Surg **123,** 192, 2009.
10. Breuing, K., Butler, C.E., Ferzoco, S., Franz, M., Hultman, C.S., Kilbridge, J.F., *et al.* Incisional ventral hernias: review of the literature and recommendations regarding the grading and technique of repair. Surgery **148,** 544, 2010.
11. Lin, S.J., and Butler, C.E. Subtotal thigh flap and bioprosthetic mesh reconstruction for large, composite abdominal wall defects. Plast Reconstr Surg **125,** 1146, 2010.
12. Baumann, D.P., and Butler, C.E. Bioprosthetic mesh in abdominal wall reconstruction. Semin Plast Surg **26,** 18, 2012.
13. Butler, C.E., and Campbell, K.T. Minimally invasive component separation with inlay bioprosthetic mesh (MICSIB) for complex abdominal wall reconstruction. Plast Reconstr Surg **128,** 698, 2011.
14. Burns, N.K., Jaffari, M.V., Rios, C.N., Mathur, A.B., and Butler, C.E. Non-cross-linked porcine acellular dermal matrices for abdominal wall reconstruction. Plast Reconstr Surg **125,** 167, 2010.
15. Butler, C.E., Burns, N.K., Campbell, K.T., Mathur, A.B., Jaffari, M.V., and Rios, C.N. Comparison of cross-linked and non-cross-linked porcine acellular dermal matrices for ventral hernia repair. J Am Coll Surg **211,** 368, 2010.
16. Campbell, K.T., Burns, N.K., Rios, C.N., Mathur, A.B., and Butler, C.E. Human versus non-cross-linked porcine acellular dermal matrix used for ventral hernia repair: comparison of *in vivo* fibrovascular remodeling and mechanical repair strength. Plast Reconstr Surg **127,** 2321, 2011.
17. Peterson, B., Zhang, J., Iglesias, R., Kabo, M., Hedrick, M., Benhaim, P., *et al.* Healing of critically sized femoral defects, using genetically modified mesenchymal stem cells from human adipose tissue. Tissue Eng **11,** 120, 2005.
18. Mizuno, H. Adipose-derived stem cells for tissue repair and regeneration: ten years of research and a literature review. J Nippon Med Sch **76,** 56, 2009.
19. Lendeckel, S., Jodicke, A., Christophis, P., Heidinger, K., Wolff, J., Fraser, J.K., *et al.* Autologous stem cells (adipose) and fibrin glue used to treat widespread traumatic calvarial defects: case report. J Craniomaxillofac Surg **32,** 370, 2004.
20. Cowan, C.M., Shi, Y.Y., Aalami, O.O., Chou, Y.F., Mari, C., Thomas, R., *et al.* Adipose-derived adult stromal cells heal critical-size mouse calvarial defects. Nat Biotechnol **22,** 560, 2004.
21. Alhadlaq, A., Tang, M., and Mao, J.J. Engineered adipose tissue from human mesenchymal stem cells maintains predefined shape and dimension: implications in soft tissue augmentation and reconstruction. Tissue Eng **11,** 556, 2005.
22. Gimble, J., and Guilak, F. Adipose-derived adult stem cells: isolation, characterization, and differentiation potential. Cytotherapy **5,** 362, 2003.
23. Gimble, J.M., Katz, A.J., and Bunnell, B.A. Adipose-derived stem cells for regenerative medicine. Circ Res **100,** 1249, 2007.
24. Gimble, J.M., and Nuttall, M.E. Adipose-derived stromal/stem cells (ASC) in regenerative medicine: pharmaceutical applications. Curr Pharm Des **17,** 332, 2011.
25. Zuk, P.A., Zhu, M., Ashjian, P., De Ugarte, D.A., Huang, J.I., Mizuno, H., *et al.* Human adipose tissue is a source of multipotent stem cells. Mol Biol Cell **13,** 4279, 2002.
26. Zuk, P.A., Zhu, M., Mizuno, H., Huang, J., Futrell, J.W., Katz, A.J., *et al.* Multilineage cells from human adipose tissue: implications for cell-based therapies. Tissue Eng **7,** 211, 2001.
27. Rigotti, G., Marchi, A., Galie, M., Baroni, G., Benati, D., Krampera, M., *et al.* Clinical treatment of radiotherapy tissue damage by lipoaspirate transplant: a healing process mediated by adipose-derived adult stem cells. Plast Reconstr Surg **119,** 1409, 2007.
28. Nakagami, H., Maeda, K., Morishita, R., Iguchi, S., Nishikawa, T., Takami, Y., *et al.* Novel autologous cell therapy in ischemic limb disease through growth factor secretion by cultured adipose tissue-derived stromal cells. Arterioscler Thromb Vasc Biol **25,** 2542, 2005.
29. Kang, S.K., Lee, D.H., Bae, Y.C., Kim, H.K., Baik, S.Y., and Jung, J.S. Improvement of neurological deficits by intracerebral transplantation of human adipose tissue-derived stromal cells after cerebral ischemia in rats. Exp Neurol **183,** 355, 2003.
30. Altman, A.M., Abdul Khalek, F.J., Alt, E.U., and Butler, C.E. Adipose tissue-derived stem cells enhance bioprosthetic mesh repair of ventral hernias. Plast Reconstr Surg **126,** 845, 2010.
31. Butler, C.E., Navarro, F.A., and Orgill, D.P. Reduction of abdominal adhesions using composite collagen-GAG implants for ventral hernia repair. J Biomed Mater Res **58,** 75, 2001.
32. Gobin, A.S., Butler, C.E., and Mathur, A.B. Repair and regeneration of the abdominal wall musculofascial defect using silk fibroin-chitosan blend. Tissue Eng **12,** 3383, 2006.
33. Davidson, J.M. Animal models for wound repair. Arch Dermatol Res **290 Suppl,** S1, 1998.
34. Oedayrajsingh-Varma, M.J., van Ham, S.M., Knippenberg, M., Helder, M.N., Klein-Nulend, J., Schouten, T.E., *et al.* Adipose tissue-derived mesenchymal stem cell yield and growth characteristics are affected by the tissue-harvesting procedure. Cytotherapy **8,** 166, 2006.
35. Yoshimura, K., Shigeura, T., Matsumoto, D., Sato, T., Takaki, Y., Aiba-Kojima, E., *et al.* Characterization of freshly isolated and cultured cells derived from the fatty and fluid portions of liposuction aspirates. J Cell Physiol **208,** 64, 2006.
36. Cao, Y., Sun, Z., Liao, L., Meng, Y., Han, Q., and Zhao, R.C. Human adipose tissue-derived stem cells differentiate into endothelial cells *in vitro* and improve postnatal neovascularization *in vivo*. Biochem Biophys Res Commun **332,** 370, 2005.
37. Acquistapace, A., Bru, T., Lesault, P.F., Figeac, F., Coudert, A.E., le Coz, O., *et al.* Human mesenchymal stem cells reprogram adult cardiomyocytes toward a progenitor-like state through partial cell fusion and mitochondria transfer. Stem Cells **29,** 812, 2011.
38. Altman, A.M., Chiu, E.S., Bai, X., Yan, Y., Song, Y.H., Newsome, R.E., *et al.* Human adipose-derived stem cells adhere to acellular dermal matrix. Aesthetic Plast Surg **32,** 698, 2008.
39. Altman, A.M., Abdul Khalek, F.J., Seidensticker, M., Pinilla, S., Yan, Y., Coleman, M., *et al.* Human tissue-resident stem cells combined with hyaluronic acid gel provide fibrovascular-integrated soft-tissue augmentation in a murine photoaged skin model. Plast Reconstr Surg **125,** 63, 2010.
40. Altman, A.M., Matthias, N., Yan, Y., Song, Y.H., Bai, X., Chiu, E.S., *et al.* Dermal matrix as a carrier for *in vivo*

delivery of human adipose-derived stem cells. Biomaterials **29,** 1431, 2008.
41. Altman, A.M., Yan, Y., Matthias, N., Bai, X., Rios, C., Mathur, A.B., *et al.* IFATS collection: human adipose-derived stem cells seeded on a silk fibroin-chitosan scaffold enhance wound repair in a murine soft tissue injury model. Stem Cells **27,** 250, 2009.
42. Singer, A.J., and Clark, R.A. Cutaneous wound healing. N Engl J Med **341,** 738, 1999.
43. Badylak, S.F., Freytes, D.O., and Gilbert, T.W. Extracellular matrix as a biological scaffold material: structure and function. Acta Biomater **5,** 1, 2009.
44. Brown, B.N., Londono, R., Tottey, S., Zhang, L., Kukla, K.A., Wolf, M.T., *et al.* Macrophage phenotype as a predictor of constructive remodeling following the implantation of biologically derived surgical mesh materials. Acta Biomater **8,** 978, 2012.
45. Brown, B.N., Valentin, J.E., Stewart-Akers, A.M., McCabe, G.P., and Badylak, S.F. Macrophage phenotype and remodeling outcomes in response to biologic scaffolds with and without a cellular component. Biomaterials **30,** 1482, 2009.
46. Gonzalez, M.A., Gonzalez-Rey, E., Rico, L., Buscher, D., and Delgado, M. Adipose-derived mesenchymal stem cells alleviate experimental colitis by inhibiting inflammatory and autoimmune responses. Gastroenterology **136,** 978, 2009.
47. Cui, L., Yin, S., Liu, W., Li, N., Zhang, W., and Cao, Y. Expanded adipose-derived stem cells suppress mixed lymphocyte reaction by secretion of prostaglandin E2. Tissue Eng **13,** 1185, 2007.
48. Wren, T.A., and Carter, D.R. A microstructural model for the tensile constitutive and failure behavior of soft skeletal connective tissues. J Biomech Eng **120,** 55, 1998.
49. Zhao, Y., Zhang, Z., Wang, J., Yin, P., Zhou, J., Zhen, M., *et al.* Abdominal hernia repair with a decellularized dermal scaffold seeded with autologous bone marrow-derived mesenchymal stem cells. Artif Organs **36,** 247, 2012.
50. Xing, L., Franz, M.G., Marcelo, C.L., Smith, C.A., Marshall, V.S., and Robson, M.C. Amnion-derived multipotent progenitor cells increase gain of incisional breaking strength and decrease incidence and severity of acute wound failure. J Burns Wounds **7,** e5, 2007.
51. Halme, D.G., and Kessler, D.A. FDA regulation of stem-cell-based therapies. N Engl J Med **355,** 1730, 2006.
52. Badylak, S., Kokini, K., Tullius, B., Simmons-Byrd, A., and Morff, R. Morphologic study of small intestinal submucosa as a body wall repair device. J Surg Res **103,** 190, 2002.

Address correspondence to:
Charles E. Butler, MD, FACS
Department of Plastic Surgery, Unit 1488
The University of Texas MD Anderson Cancer Center
P.O. Box 301402
Houston, TX 77030-1402

E-mail: cbutler@mdanderson.org

Received: April 24, 2014
Accepted: August 15, 2014
Online Publication Date: September 30, 2014